Geophysical Research Letters®

Key Points:

- Satellite data show a relative minimum in the NO_2 concentration within the Asian summer monsoon (ASM) in the upper troposphere-lower stratosphere (UTLS)
- Photochemical box model calculations show corresponding maxima in UTLS NO and NO_x, due to low O_3 and temperature in the monsoon
- NO_2 and NO_x from satellite data and a climate model show good agreement within the ASM

Tropopause-Level NO_x in the Asian Summer Monsoon

Kimberlee Dubé[1] , **William Randel[2]** , **Adam Bourassa[1]** , and **Doug Degenstein[1]**

[1]Institute of Space and Atmospheric Studies, University of Saskatchewan, Saskatoon, SK, Canada, [2]National Center for Atmospheric Research, Boulder, CO, USA

Abstract Deep convection within the Asian summer monsoon (ASM) transports surface level air into the upper troposphere-lower stratosphere (UTLS). This work aims to understand the distribution of NO_2, NO, and NO_x in the UTLS ASM anticyclone from satellite measurements. Observations of NO_2 from the Optical Spectrograph and InfraRed Imager System, the Atmospheric Chemistry Experiment - Fourier Transform Spectrometer (ACE-FTS), and the Stratospheric Aerosol and Gas Experiment III on the International Space Station are considered. The PRATMO photochemical box model is used to quantify the NO_x photochemistry, and to derive the NO_x concentration using OSIRIS NO_2 and O_3 observations. The satellite data show a relative minimum in NO_2 over the ASM in the summer months, while the corresponding NO and NO_x anomalies are elevated, mainly due to low O_3 and cold temperatures within the ASM. The observations within the ASM show reasonable agreement to simulations from the Whole Atmosphere Community Climate Model.

Plain Language Summary Motion within the Asian summer monsoon (ASM) transports air from the Earth's surface to the upper troposphere-lower stratosphere (UTLS), an altitude of around 10–15 km. This provides a pathway for surface level pollutants to influence the chemistry of the UTLS. One such pollutant is NO_x, which is the sum of NO_2 and NO. Here we consider observations of NO_2 from the Optical Spectrograph and InfraRed Imager System, the Atmospheric Chemistry Experiment-Fourier Transform Spectrometer (ACE-FTS), and the Stratospheric Aerosol and Gas Experiment III on the International Space Station, along with NO_x derived from OSIRIS NO_2 and O_3 observations. The satellite data show that a relative maximum in NO_x within the UTLS ASM corresponds to a relative minimum in NO_2. This is mainly due to low O_3 and cold temperatures within the ASM that alter the NO_x chemistry. The observations show good agreement with climate model simulations. These findings provide new information on UTLS NO_x behavior and the chemistry that occurs within the ASM.

1. Introduction

The Asian summer monsoon (ASM) is a region of persistent deep convection that appears over the southeast Asian region each summer, driving a planetary-scale anticyclonic circulation in the upper troposphere-lower stratosphere (UTLS). Important aspects of monsoon convection and circulation include the rapid transport of air from the surface into the UTLS and confinement by anticyclonic circulation (e.g., Bian et al., 2020; Bourassa et al., 2012; Brunamonti et al., 2018; Li et al., 2005; Pan et al., 2016; Randel et al., 2010; von Hobe et al., 2021). These processes provide a pathway for near-surface air, including pollutants, to influence UTLS chemical processes.

Measurements from satellite limb and occultation instruments are useful for observing the composition of the monsoon, providing complementary information to nadir-sounding satellite instruments and sparse research aircraft measurements. Numerous studies have used these satellite observations to quantify the chemical composition of the UTLS associated with the ASM, showing enhanced values of chemical constituents that originate in the troposphere, such as CO and HCN (e.g., Li et al., 2005; Park et al., 2008; Randel et al., 2010). On the other hand, O_3 and HNO_3, which are molecules of stratospheric origin, show decreased concentrations within the monsoon anticyclone (e.g., Park et al., 2007, 2008; Santee et al., 2017). The monsoon anticyclone is also associated with cold temperature anomalies in the UTLS, and warm temperature anomalies in the mid-troposphere (Randel & Park, 2006).

Nitrogen oxides NO and NO_2 (the sum of which is called NO_x) play a critical role in the chemistry of the atmosphere. In the troposphere NO_x produces O_3, while in the stratosphere NO_x destroys O_3. Roy et al. (2017) linked

increases in Chinese and Indian NO_x emissions to increased O_3 production within the troposphere during the ASM. Fadnavis et al. (2015) modeled enhanced NO_x in the ASM, which they associated with the upward transport of pollutants and the production of NO_x in the upper troposphere by lightning. Lightning is known to produce NO_x (e.g., Tie et al., 2001; Zhang et al., 2000) and the ASM has been associated with high lightning flash rates (Penki & Kamra, 2013). While Fadnavis et al. (2015) found that the transport of emissions to the UTLS is the largest factor affecting NO_x in the ASM, Lelieveld et al. (2018) found that lightning is still a key source of NO_x in the upper tropospheric monsoon anticyclone. Lelieveld et al. (2018) present the near continuous production of lightning NO_x within the ASM convection region as the key factor in the formation of upper tropospheric OH. The OH can then oxidize pollutant gases into forms that are easily removed by precipitation, thus cleansing the atmosphere.

While the above studies have focused on modeling the influence of the ASM on NO_x, comparatively little is known about the observed behavior of the individual components of NO_x, NO, and NO_2. Park et al. (2004) examined NO and NO_2 observations from the Halogen Occultation Experiment (HALOE, Russell et al., 1993). Only the HALOE sunset occultations were considered. Park et al. (2004) found that the mean July NO and NO_2 mixing ratios at 100 hPa from 1992 to 2002 both displayed maximum values in the ASM anticyclone region. When added together to get NO_x the HALOE data showed a maximum of 0.5–0.8 ppmv in the ASM. They suggested that this lower stratospheric NO_x maximum is due to the transport of tropospheric NO_x produced by lightning. Aside from Park et al. (2004), little observational evidence on the behavior of NO_x in the ASM has been reported.

Here we investigate NO_x in the ASM using NO_2 measurements from the Optical Spectrograph and InfraRed Imager System (OSIRIS, Llewellyn et al., 2004), combined with the PRATMO photochemical box model (McLinden et al., 2000). Additional satellite measurements are provided by the Atmospheric Chemistry Experiment—Fourier Transform Spectrometer (ACE-FTS, Bernath et al., 2005), and the Stratospheric Aerosol and Gas Experiment on the International Space Station (SAGE III/ISS, Cisewski et al., 2014). We include comparisons with simulations from the Whole Atmosphere Community Climate Model (WACCM, e.g., Gettelman et al., 2019) to inform the satellite data analysis and evaluate model behavior. The focus here is on temporal and spatial averages, rather than the shorter term variability that is a feature of the ASM anticyclone (e.g., Gottschaldt et al., 2018; Vogel et al., 2016). The combination of data from several instruments, along with the models, provides novel information on UTLS NO_x behavior and related photochemistry of the ASM.

2. Satellite Data and Models

2.1. OSIRIS

OSIRIS has been operating from a sun-synchronous orbit aboard the Odin satellite since October 2001 (Llewellyn et al., 2004; Murtagh et al., 2002). The optical spectrograph scans the limb of the atmosphere to measure 100 to 400 vertical profiles of limb-scattered solar irradiance each day, at wavelengths from 280 to 800 nm. Only the descending node measurements, occurring near a local solar time (LST) of 6:30 a.m., are used here. These form the vast majority of the observations throughout the mission. The exact timing of the measurements varies by about an hour due to the precessing orbit of the spacecraft.

We are using version 7.2 of the OSIRIS NO_2 retrieval, which is fully described and validated in Dubé et al. (2022). Earlier versions of the NO_2 retrieval were developed by Sioris et al. (2003), Haley et al. (2004), Bourassa et al. (2011), and Sioris et al. (2017). The v7.2 retrieval was designed to improve performance in the UTLS through improved cloud and aerosol filtering, and to reduce a low bias observed in the previous v6.0. The OSIRIS NO_2 is available for altitudes from 10.5 to 39.5 km. As we are focused on the UTLS the averaging kernel filter discussed in Dubé et al. (2022) is used here to ensure that only NO_2 values with a well-behaved averaging kernel are included in the analysis. This filter puts a lower bound on the NO_2 profiles by determining where the peak of the averaging kernel becomes more than 1.5 km different from the altitude at which information is being retrieved.

2.2. PRATMO

The PRATMO photochemical box model was initially developed by M. Prather and Jaffe (1990) and subsequently updated by McLinden et al. (2000). The reactions included in the model are listed in Logan et al. (1978)
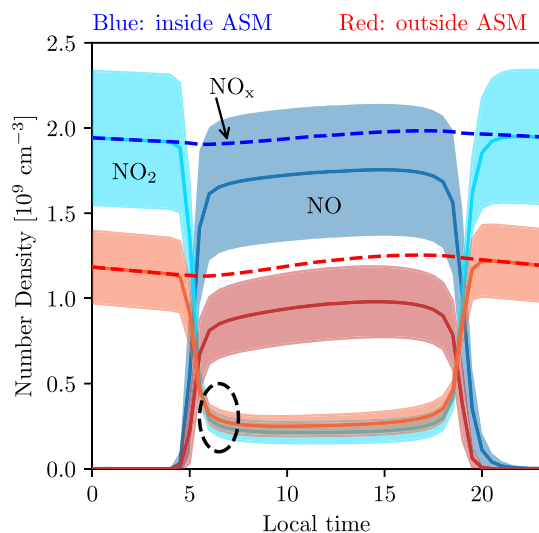
Figure 1. Mean daily cycle in NO, NO_2, and NO_x at 17.5 km calculated by PRATMO with OSIRIS inputs from July 2008, contrasting behaviors inside versus outside of the Asian summer monsoon (ASM). The shaded areas are the standard deviation. Inside the ASM is defined as 20°–40°N, 20°–120°E. Outside the ASM is defined as 20°–40°N, 180°–120°W. OSIRIS NO_2 measurements occur in the early morning, as indicated by the black dashed oval.

and McLinden et al. (2000). PRATMO starts with an input atmospheric state, then computes a set of chemical reactions over 1 day, iterating until the start and end values converge (M. J. Prather, 1992). The result is a 24 hr steady-state system of all the chemical species included in the model. The inputs required by the model are ozone, temperature, air density, and pressure profiles for a specified latitude, longitude, and date. These parameters are kept constant over the course of the day. OSIRIS measures O_3 so those values are used in the PRATMO runs. The model outputs are the NO_2 and NO profiles at any predetermined LST.

We use PRATMO results to scale the OSIRIS NO_2 observations to a common LST, and to convert the OSIRIS NO_2 to NO_x. The scaling of NO_2 measurements to a different LST is a commonly used process that accounts for variations in the measurement time due to the precessing satellite orbit (e.g., Brohede et al., 2007; Dubé et al., 2020; Park et al., 2017). Here all OSIRIS measurements are scaled to 12:00 p.m. Details of the calculation are given in Dubé et al. (2020). The OSIRIS NO_2 is converted to NO_x by multiplication with the ratio of PRATMO NO_x to NO_2, as employed previously by Park et al. (2017) and Dubé et al. (2020).

2.3. WACCM

We perform parallel analyses on simulations from WACCM, which is a comprehensive chemistry-climate model. WACCM details are discussed at https://www2.acom.ucar.edu/gcm/waccm, and we use the recently updated version 6 (WACCM6) described in Gettelman et al. (2019). The simulation used here has ∼1° horizontal resolution and 88 vertical levels from the surface to 140 km (∼1 km vertical resolution in the UTLS), and uses so-called specified dynamics (SD) incorporating meteorological fields from Modern-Era Retrospective analysis for Research and Applications Version 2 (MERRA-2) reanalyses (Gelaro et al., 2017). The kinetic reaction rates used in WACCM are from Burkholder et al. (2015). We analyze results from one monsoon season covering 15 July–30 August 2020. To analyze diurnal variability, the model output is saved at 3-hr intervals. The WACCM values were converted from UTC to LST by calculating the solar time in each latitude and longitude bin and interpolating between the 3-hourly time intervals for each day to get values at a LST of 12:00 p.m.

3. Results

3.1. Photochemistry

The NO_x number density and the proportion of NO_2 and NO that make up the NO_x both depend on the local solar time, and the balances depend on the background photochemical environment, especially O_3 and temperature. The diurnal cycles of NO_x components inside and outside of the ASM region derived from OSIRIS NO_2 measurements and PRATMO calculations are illustrated in Figure 1. There is a sharp decrease in the NO_2 concentration at sunrise as it is photolyzed to become NO via the reaction

$$NO_2 + h\nu \rightarrow NO + O. \tag{1}$$

Throughout the daylight hours NO_2 and NO are in approximate equilibrium as they interconvert rapidly through the reactions

$$NO_2 + O \rightarrow NO + O_2 \tag{2}$$

and

$$NO + O_3 \rightarrow NO_2 + O_2. \tag{3}$$

NO is the dominant daytime component of NO_x in the UTLS, mainly due to low O_3 near the tropopause (slow NO conversion from Reaction 3). At sunset Reaction 1 ceases producing NO, resulting in a rapid increase in
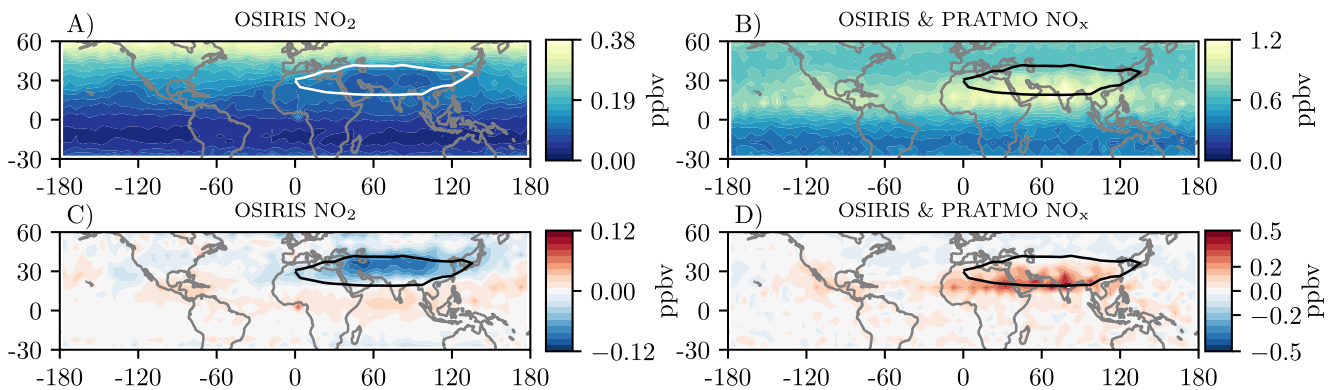
Figure 2. (a) Time average 85 hPa NO_2 in JJA for the whole OSIRIS mission, with values scaled to 12:00 p.m. (b) Mean NO_x at 85 hPa calculated from OSIRIS NO_2 and PRATMO. Corresponding longitudinal anomalies in (c) NO_2 and (d) NO_x at 85 hPa, calculated as differences from the mean values over the Pacific Ocean (180°–120°W). Circled area is the 16.75 km geopotential height contour at 100 hPa used to identify the Asian summer monsoon.

the NO_2 concentration. Overnight both the NO and NO_2 amounts decrease slowly as they are converted to nitrogen containing reservoir species (primarily NO_3 and N_2O_5). Satellite limb observations (e.g., OSIRIS) usually occur near dawn/dusk, and satellite occultation observations (including ACE-FTS and SAGE III/ISS) occur at sunrise/sunset, so the rapidly changing chemistry at these times of day needs to be considered when interpreting the satellite measurements.

As seen in Figure 1, the relative daytime NO fraction is larger inside of the ASM compared to outside. Sensitivity tests with PRATMO show that these photochemical balances are mostly linked to low O_3 in the ASM, with a secondary influence of cold temperatures (because of the temperature dependence of the rate constant in Reaction 3, e.g., Burkholder et al., 2020). For UTLS conditions, a decrease in O_3 of about 50% produces 25% less NO_2 and 5% more NO, while 4% lower temperatures result in about 4% less NO_2 and 15% more NO at 85 hPa. Both low ozone and cold temperatures are accentuated within the UTLS ASM.

While we focus here on the partitioning of NO_x between NO and NO_2, it should be noted that other nitrogen-containing compounds could also influence the overall NO_x concentration. The presence of the Asian tropopause aerosol layer (Vernier et al., 2011), along with the colder temperatures in the ASM anticyclone, provide an opportunity for enhanced heterogeneous chemistry. This could result in the conversion of NO_x to either N_2O_5 or $ClONO_2$. Solomon et al. (2016) observed enhanced heterogeneous chlorine activation in the ASM within a model simulation, and a corresponding downwind enhancement of $ClONO_2$, so the loss of NO_x through this pathway is likely to occur.

3.2. Satellite Observations

The 30-year average OSIRIS NO_2 concentration has a minima in the ASM during the summer months. Figure 2a shows the mean NO_2 volume mixing ratio (VMR) at 85 hPa in June-July-August (JJA) as measured by OSIRIS. The mean values include NO_2 observations from 2002 to 2020. Each OSIRIS NO_2 profile was interpolated from altitude to pressure levels and converted from number density to VMR using the temperature and pressure information from MERRA-2 that is included in the data files. The approximate location of the ASM is given by the 16.75 km geopotential height contour at 100 hPa (e.g., Bourassa et al., 2012).

The ASM minimum in the OSIRIS NO_2 observations is most easily seen by removing the large-scale background latitudinal structure (Figure 2c). The anomaly for a given latitude is the difference from the mean value at that latitude over the Pacific Ocean (180°–120°W), far outside of the monsoon. The NO_2 is about 0.1 ppbv lower in the ASM region that it is at other longitudes.

A test was performed to ensure that shifting the OSIRIS NO_2 observations to 12:00 p.m. using scale factors derived from O_3 and temperature inputs to PRATMO did not produce the signal observed in Figures 2a and 2c. First we calculated the zonal mean NO_2. The average PRATMO scale factor in each latitude and longitude bin was then used to scale the zonal mean NO_2 to noon. This scaling did not produce significant longitudinal structure that could be associated with the ASM, providing confidence that the ASM signal in the OSIRIS NO_2 observations is real, rather than produced by PRATMO.
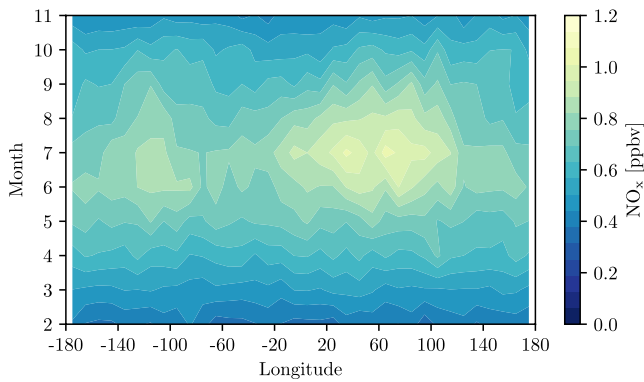
Figure 3. Monthly average 85 hPa NO_x as a function of longitude derived from OSIRIS + PRATMO calculations (scaled to 12:00). Data are averaged over 20°–40°N.

Figure 2b shows the corresponding time average NO_x derived from OSIRIS NO_2 and PRATMO, also scaled to 12:00 p.m. local time. The calculated NO_x is substantially higher than NO_2 at all longitudes, consistent with Figure 1. NO_x is relatively high in the monsoon region, as highlighted by removing the background latitudinal structure in Figure 2d. The opposite signed NO_2 and NO_x anomalies in Figure 2 are explained by the photochemical balances shown in Figure 1, with the result that NO and NO_x are enhanced inside the ASM during the daytime, while NO_2 is reduced. This behavior is mainly tied to the low O_3 and low temperatures observed in the ASM.

The monthly evolution of 85 hPa NO_x from the OSIRIS + PRATMO calculations (Figure 3) shows elevated NO_x from May to September extending over 0°–120°E. This seasonal variation and longitudinal maximum are clear signatures of links to the ASM during summer. Figure 3 also shows a smaller region of elevated NO_x from about 80° to 140°W, which could indicate an influence of the North American monsoon on the UTLS (also seen in Figure 2d).

We have also examined corresponding NO_2 behavior from SAGE III/ISS and ACE-FTS sunset occultations. Time average anomalies in NO_2 from both ACE-FTS and SAGE III/ISS are negative within the ASM region (Figure S1 in Supporting Information S1), as they are for OSIRIS (Figure 2c). The daily photochemical cycle in NO_2 (Section 3.1) makes it challenging to perform quantitative comparisons to OSIRIS. Measurements at the terminator cannot be accurately scaled to a different local solar time because the radiative transfer in PRATMO uses a simplified plane-parallel atmosphere. This prevents modeling NO_2 and NO at the terminator with the precision required for the rapidly changing conditions. The ACE-FTS NO has a maximum within the ASM anticyclone (bottom panel of Figure S1 in Supporting Information S1), despite having large uncertainties at this pressure level. At sunset, the balance of NO and NO_2 starts to switch so there is less NO than NO_2, which is why the ACE-FTS NO anomaly is smaller than the NO_2 anomaly.

3.3. WACCM Simulations

The WACCM time average NO_2, NO, and NO_x anomalies are in good agreement with those from the satellite instruments. Figure 4 shows the WACCM output at 85 hPa and 12:00 p.m. The NO_2 anomaly is low in the ASM region, as it is for each of OSIRIS, ACE-FTS, and SAGE III/ISS. The WACCM NO anomaly has a maxima in the ASM that is substantially larger than the NO_2 minimum. The corresponding WACCM NO_x has an ASM maximum that is similar in sign and magnitude to the NO_x derived from the OSIRIS + PRATMO calculations (Figure 2d).

The vertical structure of the monsoon NO_x behavior from OSIRIS observations and WACCM are compared in Figure 5, which shows the percent differences for the NO_2 and NO_x inside versus outside of the ASM as a function of pressure level. Percent differences are used to highlight UTLS vertical structure and de-emphasize the background NO_x increase with altitude in the stratosphere. We additionally include the corresponding O_3 difference profiles in Figure 5 because of their importance in the NO_x balances; these show the well-known reduced UTLS O_3 within the ASM (e.g., Park et al., 2007, 2008), with somewhat larger anomalies in OSIRIS compared to WACCM. Both the OSIRIS and WACCM results show negative anomalies in NO_2 within the ASM extending from ~100 to 60 hPa. The maximum relative NO_2 difference occurs at the 85 hPa level, overlapping the large negative ozone anomalies within the ASM.

The NO_x anomaly is positive for both OSIRIS + PRATMO and WACCM throughout the UTLS region. ASM NO_x anomalies near the tropopause are ~25% inside larger than outside, with bigger relative anomalies at lower altitudes (in WACCM). Hence the satellite measurements (above ~100 hPa) are observing the top of the ASM. Overall, there is reasonable quantitative agreement between the observations and model simulation in terms of profile shape and magnitude.
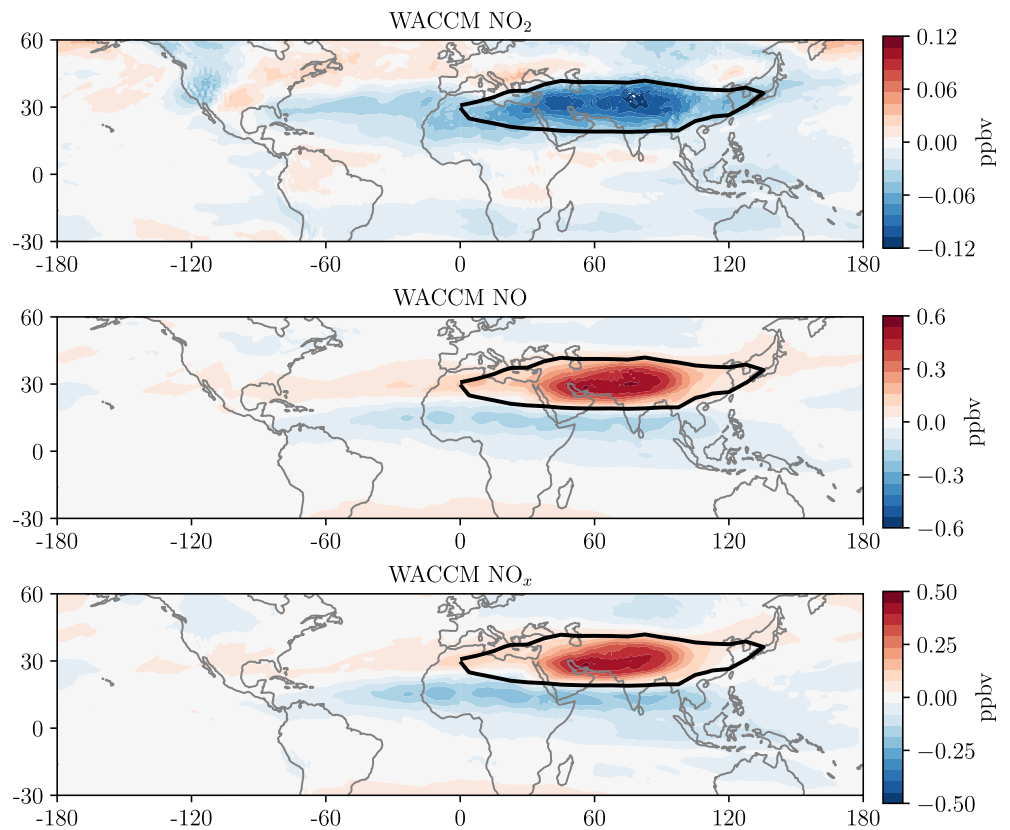
Figure 4. Whole Atmosphere Community Climate Model time average NO, NO_2, and NO_x at 85 hPa from July 15 to 30 August 2020. Values were interpolated to a local time of 12:00 p.m. in each bin. The anomaly at each latitude is the difference from the mean value at that latitude over the Pacific ocean (180°–120°W). Circled area is the 16.75 km geopotential height contour at 100 hPa.
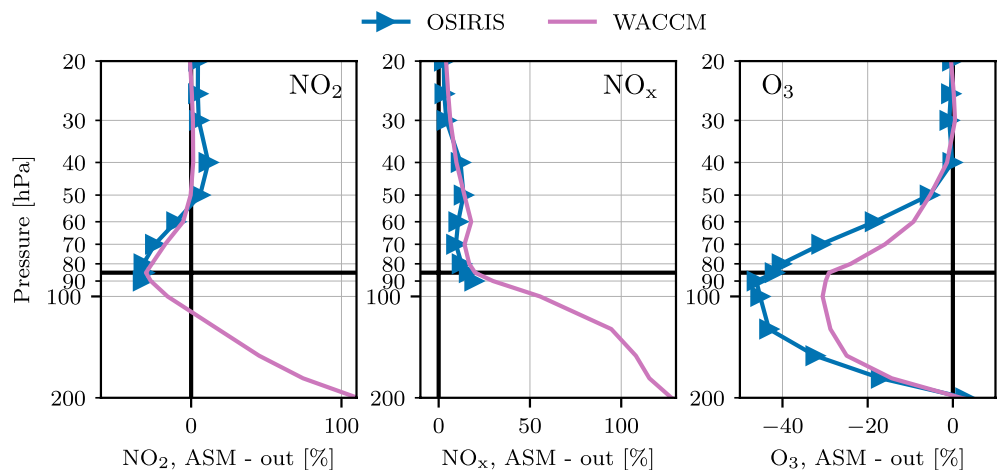
Figure 5. Vertical profiles of JJA anomalies in NO_2, NO_x, and O_3 inside versus outside the Asian summer monsoon for OSIRIS and Whole Atmosphere Community Climate Model (WACCM). Results are shown in terms of local percentage anomalies. The Asian monsoon region is defined as inside the 16.75 km WACCM geopotential height contour at 100 hPa, while the outside monsoon region is defined as 20°–40°N, 180°–120°W. NO_2 and NO_x results are for 12:00 p.m. The black horizontal line marks the 85 hPa level used in the other figures.

4. Conclusion

The influence of the ASM anticyclone on NO_2, NO, and NO_x was investigated using observations from OSIRIS, SAGE III/ISS, and ACE-FTS, along with the PRATMO box model and chemistry-climate model output from WACCM. While the OSIRIS, SAGE III/ISS and ACE-FTS data show a relative minimum in NO_2 near the tropopause within the ASM, the PRATMO calculations show enhanced NO and NO_x in the monsoon. The enhanced NO_x within the monsoon region derived from satellite observations agrees quantitatively with chemistry-climate model simulations from WACCM, including chemical isolation within the anticyclone and consistent vertical profiles. The enhanced NO_x levels in the UTLS ASM likely result from a combination of upwards transport of surface level pollutants and production by lightning, as shown in modeling studies (e.g., Fadnavis et al., 2015; Lelieveld et al., 2018; Roy et al., 2017). Here we find that the low background O_3 amounts and cold temperatures in the UTLS, which are accentuated in the ASM, shift the daytime NO_x balances toward enhanced NO and reduced NO_2. The satellite observations presented here provide a method to evaluate NO_x behavior in chemistry-climate models.

Data Availability Statement

OSIRIS data, including the PRATMO derived NO_x and values scaled to noon, are available at ftp://odin-osiris.usask.ca/OSIRIS/Level2/. SAGE III/ISS NO_2 data accounting for diurnal variations along the line of sight are available at ftp://odin-osiris.usask.ca/SAGEIII_ISS. The WACCM results are available at ftp://odin-osiris.usask.ca/Models. Instructions for downloading the OSIRIS, SAGE III/ISS and WACCM files are at https://research-groups.usask.ca/osiris/data-products.php#Download. ACE data are available by signing up at https://databace.scisat.ca/l2signup.php. The PRATMO python package can be downloaded from https://arg.usask.ca/wheels/ and documentation is available at https://arg.usask.ca/docs/Pratmo/pratmo_boxmodel.html. The WACCM model is available at https://www.cesm.ucar.edu/models/cesm2/.

References

Bernath, P. F., McElroy, C. T., Abrams, M. C., Boone, C. D., Butler, M., Camy-Peyret, C., et al. (2005). Atmospheric chemistry experiment (ACE): Mission overview. *Geophysical Research Letters*, *32*(15), L15S01. https://doi.org/10.1029/2005GL022386

Bian, J., Li, D., Bai, Z., Li, Q., Lyu, D., & Zhou, X. (2020). Transport of Asian surface pollutants to the global stratosphere from the Tibetan Plateau region during the Asian summer monsoon. *National Science Review*, *7*(3), 516–533. https://doi.org/10.1093/nsr/nwaa005

Bourassa, A. E., McLinden, C. A., Sioris, C. E., Brohede, S., Bathgate, A. F., Llewellyn, E. J., & Degenstein, D. A. (2011). Fast NO_2 retrievals from Odin-OSIRIS limb scatter measurements. *Atmospheric Measurement Techniques*, *4*(5), 965–972. https://doi.org/10.5194/amt-4-965-2011

Bourassa, A. E., Robock, A., Randel, W. J., Deshler, T., Rieger, L. A., Lloyd, N. D., et al. (2012). Large volcanic aerosol load in the stratosphere linked to Asian monsoon transport. *Science*, *337*(6090), 78–81. https://doi.org/10.1126/science.1219371

Brohede, S. M., Haley, C. S., Mclinden, C. A., Sioris, C. E., Murtagh, D. P., Petelina, S. V., et al. (2007). Validation of Odin/OSIRIS stratospheric NO_2 profiles. *Journal of Geophysical Research*, *112*(D7), D07310. https://doi.org/10.1029/2006JD007586

Brunamonti, S., Jorge, T., Oelsner, P., Hanumanthu, S., Singh, B. B., Kumar, K. R., et al. (2018). Balloon-borne measurements of temperature, water vapor, ozone and aerosol backscatter on the southern slopes of the Himalayas during StratoClim 2016–2017. *Atmospheric Chemistry and Physics*, *18*(21), 15937–15957. https://doi.org/10.5194/acp-18-15937-2018

Burkholder, J. B., Sander, S. P., Abbatt, J., Barker, J. R., Cappa, C., Crounse, J. D., et al. (2020). *Chemical kinetics and photochemical data for use in atmospheric studies, evaluation* (Vol. 19). JPL Publication 19-5. Retrieved from https://jpldataeval.jpl.nasa.gov/

Burkholder, J. B., Sander, S. P., Abbatt, J. P. D., Barker, J. R., Huie, R. E., Kolb, C. E., et al. (2015). *Chemical kinetics and photochemical data for use in atmospheric studies, evaluation* (Vol. 19). JPL Publication 19-5. Retrieved from https://jpldataeval.jpl.nasa.gov/

Cisewski, M., Zawodny, J., Gasbarre, J., Eckman, R., Topiwala, N., Rodriguez-Alvarez, O., et al. (2014). The stratospheric aerosol and gas experiment (SAGE III) on the International Space station (ISS) mission. In *Sensors, Systems, and Next-Generation Satellites XVIII* (Vol. 9241, p. 924107). https://doi.org/10.1117/12.2073131

Dubé, K., Randel, W., Bourassa, A., Zawada, D., McLinden, C., & Degenstein, D. (2020). Trends and variability in stratospheric NO_x derived from merged SAGE II and OSIRIS satellite observations. *Journal of Geophysical Research: Atmospheres*, *125*(7), e2019JD031798. https://doi.org/10.1029/2019JD031798

Dubé, K., Zawada, D., Bourassa, A., Degenstein, D., Randel, W., Flittner, D., et al. (2022). An improved OSIRIS NO_2 profile retrieval in the UTLS and intercomparison with ACE-FTS and SAGE III/ISS. *Atmospheric Measurement Techniques Discussions*, *2022*, 1–22. https://doi.org/10.5194/amt-2022-133

Fadnavis, S., Semeniuk, K., Schultz, M. G., Kiefer, M., Mahajan, A., Pozzoli, L., & Sonbawane, S. (2015). Transport pathways of peroxyacetyl nitrate in the upper troposphere and lower stratosphere from different monsoon systems during the summer monsoon season. *Atmospheric Chemistry and Physics*, *15*(20), 11477–11499. https://doi.org/10.5194/acp-15-11477-2015

Gelaro, R., McCarty, W., Suárez, M. J., Todling, R., Molod, A., Takacs, L., et al. (2017). The modern-era retrospective analysis for research and applications, version 2 (MERRA-2). *Journal of Climate*, *30*(14), 5419–5454. https://doi.org/10.1175/JCLI-D-16-0758.1

Gettelman, A., Mills, M., Kinnison, D., Garcia, R., Smith, A., Marsh, D., et al. (2019). The whole atmosphere community climate model version 6 (WACCM6). *Journal of Geophysical Research: Atmospheres*, *124*(23), 12380–12403. https://doi.org/10.1029/2019jd030943

Gottschaldt, K.-D., Schlager, H., Baumann, R., Cai, D. S., Eyring, V., Graf, P., et al. (2018). Dynamics and composition of the Asian summer monsoon anticyclone. *Atmospheric Chemistry and Physics*, *18*(8), 5655–5675. https://doi.org/10.5194/acp-18-5655-2018

Haley, C. S., Brohede, S. M., Sioris, C. E., Griffioen, E., Murtagh, D. P., McDade, I. C., et al. (2004). Retrieval of stratospheric O_3 and NO_2 profiles from Odin Optical Spectrograph and Infrared Imager System (OSIRIS) limb-scattered sunlight measurements. *Journal of Geophysical Research*, *109*(D16), D16303. https://doi.org/10.1029/2004JD004588

Lelieveld, J., Bourtsoukidis, E., Brühl, C., Fischer, H., Fuchs, H., Harder, H., et al. (2018). The South Asian monsoon: Pollution pump and purifier. *Science*, *361*(6399), 270–273. https://doi.org/10.1126/science.aar2501

Li, Q., Jiang, J. H., Wu, D. L., Read, W. G., Livesey, N. J., Waters, J. W., et al. (2005). Convective outflow of South Asian pollution: A global CTM simulation compared with EOS MLS observations. *Geophysical Research Letters*, *32*(14). https://doi.org/10.1029/2005GL022762

Llewellyn, E. J., Lloyd, N. D., Degenstein, D. A., Gattinger, R. L., Petelina, S. V., Bourassa, A. E., et al. (2004). The OSIRIS instrument on the Odin spacecraft. *Canadian Journal of Physics*, *82*(6), 411–422. https://doi.org/10.1139/p04-005

Logan, J. A., Prather, M. J., Wofsy, S. C., McElroy, M. B., & Bates, D. R. (1978). Atmospheric chemistry: Response to human influence. *Philosophical Transactions of the Royal Society of London - Series A: Mathematical and Physical Sciences*, *290*(1367), 187–234. https://doi.org/10.1098/rsta.1978.0082

McLinden, C. A., Olsen, S. C., Hannegan, B., Wild, O., Prather, M. J., & Sundet, J. (2000). Stratospheric ozone in 3-D models: A simple chemistry and the cross-tropopause flux. *Journal of Geophysical Research*, *105*(D11), 14653–14665. https://doi.org/10.1029/2000JD900124

Murtagh, D., Frisk, U., Merino, F., Ridal, M., Jonsson, A., Stegman, J., et al. (2002). An overview of the Odin atmospheric mission. *Canadian Journal of Physics*, *80*(4), 309–319. https://doi.org/10.1139/p01-157

Pan, L. L., Honomichl, S. B., Kinnison, D. E., Abalos, M., Randel, W. J., Bergman, J. W., & Bian, J. (2016). Transport of chemical tracers from the boundary layer to stratosphere associated with the dynamics of the Asian summer monsoon. *Journal of Geophysical Research: Atmospheres*, *121*(23), 14–159. https://doi.org/10.1002/2016jd025616

Park, M., Randel, W. J., Emmons, L. K., Bernath, P. F., Walker, K. A., & Boone, C. D. (2008). Chemical isolation in the Asian monsoon anticyclone observed in Atmospheric Chemistry Experiment (ACE-FTS) data. *Atmospheric Chemistry and Physics*, *8*(3), 757–764. https://doi.org/10.5194/acp-8-757-2008

Park, M., Randel, W. J., Gettelman, A., Massie, S. T., & Jiang, J. H. (2007). Transport above the Asian summer monsoon anticyclone inferred from Aura Microwave Limb Sounder tracers. *Journal of Geophysical Research*, *112*(D16), D16309. https://doi.org/10.1029/2006JD008294

Park, M., Randel, W. J., Kinnison, D. E., Bourassa, A. E., Degenstein, D. A., Roth, C. Z., et al. (2017). Variability of stratospheric reactive nitrogen and ozone related to the QBO. *Journal of Geophysical Research: Atmospheres*, *122*(18), 10103–10118. https://doi.org/10.1002/2017JD027061

Park, M., Randel, W. J., Kinnison, D. E., Garcia, R. R., & Choi, W. (2004). Seasonal variation of methane, water vapor, and nitrogen oxides near the tropopause: Satellite observations and model simulations. *Journal of Geophysical Research*, *109*(D3). https://doi.org/10.1029/2003JD003706

Penki, R. K., & Kamra, A. K. (2013). Lightning distribution with respect to the monsoon trough position during the Indian summer monsoon season. *Journal of Geophysical Research: Atmospheres*, *118*(10), 4780–4787. https://doi.org/10.1002/jgrd.50382

Prather, M., & Jaffe, A. H. (1990). Global impact of the Antarctic ozone hole: Chemical propagation. *Journal of Geophysical Research*, *95*(D4), 3473–3492. https://doi.org/10.1029/JD095iD04p03473

Prather, M. J. (1992). Catastrophic loss of stratospheric ozone in dense volcanic clouds. *Journal of Geophysical Research*, *97*(D9), 10187–10191. https://doi.org/10.1029/92JD00845

Randel, W. J., & Park, M. (2006). Deep convective influence on the Asian summer monsoon anticyclone and associated tracer variability observed with Atmospheric Infrared Sounder (AIRS). *Journal of Geophysical Research*, *111*(D12), D12314. https://doi.org/10.1029/2005JD006490

Randel, W. J., Park, M., Emmons, L., Kinnison, D., Bernath, P., Walker, K. A., et al. (2010). Asian Monsoon transport of pollution to the stratosphere. *Science*, *328*(5978), 611–613. https://doi.org/10.1126/science.1182274

Roy, C., Fadnavis, S., Müller, R., Ayantika, D. C., Ploeger, F., & Rap, A. (2017). Influence of enhanced Asian NO_x emissions on ozone in the upper troposphere and lower stratosphere in chemistry–climate model simulations. *Atmospheric Chemistry and Physics*, *17*(2), 1297–1311. https://doi.org/10.5194/acp-17-1297-2017

Russell, J. M., III, Gordley, L. L., Park, J. H., Drayson, S. R., Hesketh, W. D., Cicerone, R. J., et al. (1993). The Halogen occultation experiment. *Journal of Geophysical Research*, *98*(D6), 10777–10797. https://doi.org/10.1029/93JD00799

Santee, M. L., Manney, G. L., Livesey, N. J., Schwartz, M. J., Neu, J. L., & Read, W. G. (2017). A comprehensive overview of the climatological composition of the Asian summer monsoon anticyclone based on 10 years of Aura Microwave Limb Sounder measurements. *Journal of Geophysical Research: Atmospheres*, *122*(10), 5491–5514. https://doi.org/10.1002/2016JD026408

Sioris, C. E., Haley, C. S., McLinden, C. A., von Savigny, C., McDade, I. C., McConnell, J. C., et al. (2003). Stratospheric profiles of nitrogen dioxide observed by Optical Spectrograph and Infrared Imager System on the Odin satellite. *Journal of Geophysical Research*, *108*(D7), 4215. https://doi.org/10.1029/2002JD002672

Sioris, C. E., Rieger, L. A., Lloyd, N. D., Bourassa, A. E., Roth, C. Z., Degenstein, D. A., et al. (2017). Improved OSIRIS NO_2 retrieval algorithm: Description and validation. *Atmospheric Measurement Techniques*, *10*(3), 1155–1168. https://doi.org/10.5194/amt-10-1155-2017

Solomon, S., Kinnison, D., Garcia, R. R., Bandoro, J., Mills, M., Wilka, C., et al. (2016). Monsoon circulations and tropical heterogeneous chlorine chemistry in the stratosphere. *Geophysical Research Letters*, *43*(24), 12624–12633. https://doi.org/10.1002/2016GL071778

Tie, X., Zhang, R., Brasseur, G., Emmons, L., & Lei, W. (2001). Effects of lightning on reactive nitrogen and nitrogen reservoir species in the troposphere. *Journal of Geophysical Research*, *106*(D3), 3167–3178. https://doi.org/10.1029/2000JD900565

Vernier, J.-P., Thomason, L. W., & Kar, J. (2011). CALIPSO detection of an Asian tropopause aerosol layer. *Geophysical Research Letters*, *38*(7), L07804. https://doi.org/10.1029/2010GL046614

Vogel, B., Günther, G., Müller, R., Grooß, J.-U., Afchine, A., Bozem, H., et al. (2016). Long-range transport pathways of tropospheric source gases originating in Asia into the northern lower stratosphere during the Asian monsoon season 2012. *Atmospheric Chemistry and Physics*, *16*(23), 15301–15325. https://doi.org/10.5194/acp-16-15301-2016

von Hobe, M., Ploeger, F., Konopka, P., Kloss, C., Ulanowski, A., Yushkov, V., et al. (2021). Upward transport into and within the Asian monsoon anticyclone as inferred from stratoclim trace gas observations. *Atmospheric Chemistry and Physics*, *21*(2), 1267–1285. https://doi.org/10.5194/acp-21-1267-2021

Zhang, R., Sanger, N. T., Orville, R. E., Tie, X., Randel, W., & Williams, E. R. (2000). Enhanced NO_x by lightning in the upper troposphere and lower stratosphere inferred from the UARS Global NO_2 measurements. *Geophysical Research Letters*, *27*(5), 685–688. https://doi.org/10.1029/1999GL010903

References From the Supporting Information

Boone, C. D., Bernath, P. F., Cok, D., Jones, S. C., & Steffen, J. (2020). Version 4 retrievals for the atmospheric chemistry experiment Fourier transform spectrometer (ACE-FTS) and imagers. *Journal of Quantitative Spectroscopy and Radiative Transfer*, *247*, 106939. https://doi.org/10.1016/j.jqsrt.2020.106939

Boone, C. D., Walker, K. A., & Bernath, P. F. (2013). Version 3 retrievals for the atmospheric chemistry experiment Fourier transform spectrometer (ACE-FTS). In P. Bernath (Ed.), *The atmospheric chemistry experiment ACE at 10: A solar occultation anthology* (Vol. 10, pp. 103–127). A. Deepak Publishing.

Dubé, K., Bourassa, A., Zawada, D., Degenstein, D., Damadeo, R., Flittner, D., & Randel, W. (2021). Accounting for the photochemical variation in stratospheric NO_2 in the SAGE III/ISS solar occultation retrieval. *Atmospheric Measurement Techniques*, *14*(1), 557–566. https://doi.org/10.5194/amt-14-557-2021

SAGE III Algorithm Theoretical Basis Document, T. (2002). SAGE III algorithm theoretical basis document (ATBD) solar and lunar algorithm (Technical Report). *LaRC 475-00-109*. Retrieved from https://eospso.gsfc.nasa.gov/sites/default/files/atbd/atbd-sage-solar-lunar.pdf

Sheese, P. E., Walker, K. A., Boone, C. D., McLinden, C. A., Bernath, P. F., Bourassa, A. E., et al. (2016). Validation of ACE-FTS version 3.5 NO_y species profiles using correlative satellite measurements. *Atmospheric Measurement Techniques*, *9*(12), 5781–5810. https://doi.org/10.5194/amt-9-5781-2016